The Tumor-Associated Calcium Signal Transducer 2 (TACSTD2) oncogene is upregulated in pre-cystic epithelial cells revealing a new target for polycystic kidney disease

Short Title: Early cyst initiators in Pkd2 mice

Abigail O. Smith[1,2+ID], William Tyler Frantz[1,2+ID], Kenley M. Preval[1,2 ID], Yvonne J.K. Edwards[1], Craig J. Ceol[1 ID], Julie A. Jonassen[3 ID] and Gregory J. Pazour[1*ID]

[1]Program in Molecular Medicine, University of Massachusetts Chan Medical School, Biotech II, Suite 213, 373 Plantation Street, Worcester, MA, USA 01605

[2]Morningside Graduate School of Biological Sciences, University of Massachusetts Chan Medical School, 55 Lake Avenue North, Worcester MA 01655

[3]Department of Microbiology and Physiological Systems, University of Massachusetts Chan Medical School, 55 Lake Avenue North, Worcester MA 01655

[+]These authors contributed equally to this work

*Correspondence to: Telephone: 508 856 8078, Email: gregory.pazour@umassmed.edu

ID

AOS: https://orcid.org/0000-0003-2765-8737
WTF: https://orcid.org/0000-0003-1207-9652
KMP: https://orcid.org/0000-0002-2425-0878
CJC: https://orcid.org/0000-0002-7188-7580
YJKE: https://orcid.org/0000-0001-8505-3168
JAJ: https://orcid.org/0000-0001-9997-2069
GJP: https://orcid.org/0000-0002-6285-8796

Abbreviations:

ADPKD, autosomal dominant polycystic kidney disease;
CIC, cyst initiation candidate;
DAPI, 4',6-diamidino-2-phenylindole;
DBA, Dolichos biflorus agglutinin;
H&E, Hematoxylin and eosin;
Tacstd2/TACSTD2, tumor-associated calcium signal transducer 2;
LTA, Lotus tetragonolobus agglutinin;
PKD, polycystic kidney disease; Pkd1/PKD1, polycystin-1; Pkd2/PKD2, polycystin-2;

One Sentence Summary

The oncogene, tumor-associated calcium signal transducer 2 (Tacstd2) mRNA increased in abundance shortly after Pkd2 loss and may be a driver of cyst initiation in polycystic kidney disease.

Abstract

Polycystic kidney disease (PKD) is an important cause of end stage renal disease, but treatment options are limited. While later stages of the disease have been extensively studied, mechanisms driving the initial conversion of renal tubules into cysts are not understood. To identify factors that promote the initiation of cysts we deleted polycystin-2 (*Pkd2*) in mice and surveyed transcriptional changes before and immediately after cysts developed. We identified 74 genes which we term cyst initiation candidates (CICs). To identify conserved changes with relevance to human disease we compared these murine CICs to single cell transcriptomic data derived from patients with PKD and from healthy controls. Tumor-associated calcium signal transducer 2 (*Tacstd2*) stood out as an epithelial-expressed gene whose levels were elevated prior to cystic transformation and further increased with disease progression. Human tissue biopsies and organoids show that TACSTD2 protein is low in normal kidney cells but is elevated in cyst lining cells. While TACSTD2 has not been studied in PKD, it has been studied in cancer where it is highly expressed in solid tumors while showing minimal expression in normal tissue. This property is being exploited by antibody drug conjugates that target TACSTD2 for the delivery of cytotoxic drugs. Our finding that Tacstd2 is highly expressed in cysts, but not normal tissue, suggests that it should be explored as a candidate for drug development in PKD. More immediately, our work suggests that PKD patients undergoing TACSTD2 treatment for cancer should be monitored for kidney effects.

Introduction

Autosomal Dominant Polycystic Kidney Disease (ADPKD) is an inherited, progressive disease in which large, fluid-filled cysts grow in both kidneys, ultimately destroying organ function. It is relatively common, affecting approximately 1 in 1,000 people (1-3). ADPKD typically results from inactivating mutations in either of two transmembrane proteins, polycystin-1 (PKD1 in humans, Pkd1 in mice) or polycystin-2 (PKD2/Pkd2). The precise function of these channel-like

proteins is unknown, but they are thought to regulate proliferation and differentiation to maintain tubular architecture. Numerous pathways downstream of the polycystins have been identified including cAMP signaling, which is the basis of Tolvaptan, the only approved FDA-approved drug therapy for ADPKD(4,5). Nonetheless, most patients require dialysis or kidney transplant by late adulthood after reaching end stage renal disease (6).

While ADPKD is categorized as an adult disease (7), cyst formation begins *in utero* and continues throughout an individual's lifespan. Adolescents may experience early symptoms of hypertension and pain, and symptom prevalence increases with age and cyst burden despite preserved kidney function (8,9). Ultimately cyst burden overwhelms kidney function, leading to end stage renal disease.

While the later stages of the disease have been extensively studied, there has been limited research into the early stages of ADPKD, including the mechanism of cyst initiation. Identifying drivers of cyst formation could provide additional therapeutic targets. In this work we used RNA sequencing to detect the earliest transcriptional changes after *Pkd2* deletion in mouse. We identified 74 genes that may drive cyst initiation, which we term cyst initiation candidates (CICs). Cross-referencing CICs with published data from pre-cystic mouse models and single-cell RNA sequence from murine and human kidneys pointed to *Tacstd2/TACSTD2*, also known as *Trop2*. While unstudied in the context of ADPKD, *TACSTD2* is highly expressed in metastatic breast cancer and other epithelial tumors. It is targeted by Sacituzumab govitecan (Trodelvy), an antibody-drug conjugate as a treatment for aggressive cancer (10). Tacstd2 antibodies strongly label small cysts in both human and mouse kidneys with minimal label in non-cystic tubules indicating that this protein should be explored as a therapeutic target.

Results

Identifying early transcriptional changes after *Pkd2* deletion

To distinguish the earliest transcriptional changes downstream of the loss of *Pkd2* function we utilized a conditionally inducible mouse model (11) (Fig 1). After intraperitoneal tamoxifen injection at postnatal day 2 (P2), control (*Cagg-Cre*^{ER}, *Pkd2*$^{flox/+}$ or *Pkd2*$^{flox/null}$, [no cre]) and experimental (*Cagg-Cre*^{ER}, *Pkd2*$^{flox/null}$) kidneys were studied at P6 and P10 (Fig 1B-C), and P14-15 (Fig 1C). The two-kidney to bodyweight ratio (2K:BW), which is a proxy for cystic burden, was

not significantly different between experimental and control animals at P6, but by P10 2K:BW was significantly elevated in the experimental animals and was further elevated in P14-15 experimental animals (Fig 1C). Consistent with the 2K:BW, H&E staining revealed no gross differences in kidney architecture in P6 experimental kidneys (Fig 1B), but cysts were evident in the P10 experimental kidneys (Fig 1B). At P10, experimental collecting ducts (marked by Aquaporin-2) were dilated or cystic whereas collecting ducts appeared normal in P6 experimental kidneys (Fig 1D).

To identify potential drivers of cyst formation, RNA was isolated from P6 and P10 experimental and control kidneys. mRNA and small RNA libraries were generated, sequenced, and analyzed by standard pipelines to identify transcriptional changes (Table 1, Fig 1A). For mRNA, differentially expressed genes (DEGs) were defined as having a false discovery rate (FDR) of less than 0.05. At P6 there were 91 DEGs (59 increased expression and 32 decreased expression) (Table S1, Fig 2A). At P10 there were 5,309 DEGs (2,645 increased expression and 2,664 decreased expression) (Table S2, Fig 2B). *Pkd2* mRNA was significantly reduced at both time points, validating our inducible Cre system. The large difference between the number of DEGs at P10 vs P6 likely corresponds to the observed rapid cyst development within this time frame. We predicted that many DEGs at P10 would represent more general cystic changes, rather than primary cyst initiation factors. Indeed, Kyoto Encyclopedia of Genes and Genomes (KEGG) enrichment analysis revealed that DEGs from P10 are primarily from proliferative programs, likely reflective of downstream targets and not novel selective targetable changes (Fig S2A). P6 differences, although fewer and of smaller magnitude than P10, are more likely to represent factors that promote cyst initiation. Gene ontology analysis did not identify significant terms for the P6 DEGs. Therefore, rather than investigating a broad pathway or biological function, we turned to the commonalities between P6 and P10 DEGs. We theorized that persistence from P6 to P10 during cyst development strengthens the possibility that the genes participate in cyst initiation. We identified 74 genes in the intersection between P6 and P10 DEGs. We defined this list as cyst initiation candidates (CICs) (Fig 2C, D). The vast majority of CICs are regulated in the same direction at P6 and P10, suggesting that the changes detected at P6 increase with cyst development (Fig 2D).

There were no differentially expressed miRNAs in the P6 dataset that reached significance (FDR < 0.05). At this early pre-cystic time point any differences in miRNA expression are likely subtle and below the level of detection by bulk sequencing. Nevertheless, we found 39 stem-loop and mature miRNAs with FDR < 0.05 at P10 (Fig S1A). 24 of the 39 genes were previously cited in PKD literature (Fig S1B), further validating our ability to detect relevant changes in small RNA expression between experimental and control kidneys. The most significantly elevated miRNA, mir-551b, is implicated in abnormal cell differentiation and proliferation in gastric cancer (12) and ovarian cancer (13). Mir-551b may warrant further study in relation to PKD pathogenesis. However, the remainder of this study focuses on mRNAs with differential expression in pre-cystic kidneys as novel candidates for cyst initiation.

Exploring cyst initiation candidates in published RNAseq datasets

To further identify the CICs most likely to drive early cystic transformation we leveraged existing data from the field. We reasoned that strong cyst initiators would be present in alternative mouse models of early PKD. Therefore, we compared our data to models differing in Cre expression, target gene (*Pkd2* vs. *Pkd1*), age and method of induction, age at sacrifice, cyst burden at time of collection, and number of mice used for analysis (Table 2). Woo *et al.* looked at disease progression in young mice at P1, P3 and P7 where *Pkd1* or *Pkd2* had been deleted during development of the collecting duct with *HoxB7-Cre* (14). This study observed few significant transcriptomic changes at the earliest time points after polycystin inactivation and the changes observed did not correlate strongly with our DEGs (Fig S2B, S2C). However, two other studies, Kunnen *et al.* and Zhang *et al.* correlated significantly with our data at P6 and P10 (Fig 2E, S2B, S2C). Importantly, we observed overall agreement in pre-cystic kidneys even between *Pkd2* and *Pkd1* models and juvenile and mature mice, suggesting that CICs may act broadly to induce cysts.

Cyst initiation candidates in human disease

To focus on the genes most relevant to human disease, we identified CICs with conserved expression patterns by reanalyzing Muto *et al.'s* (15) single cell data derived from healthy and ADPKD human kidneys. The Muto *et al.* data was re-calculated and cell types assigned according to consensus markers from Chen *et al.* (Fig 3A). To compare transcriptional

differences present in human disease, we first pseudo bulked Muto et al.'s data to identify differentially expressed genes and then compared these genes to our list of 74 CICs (Fig 3B). We found 30 DEGs in common between the human data and our list of CICs. The majority agreed in direction between human disease and our early cystic murine model. Others (such as CDKL1) demonstrated differential expressions in directions counter to our observations (Fig 3B). These genes may still represent initiator events as the human data samples end stage ADPKD, which represents a different environment than cyst initiation.

CICs that drive initial cyst growth are likely to be expressed in epithelial cells as these are sites of the first pathology in cystic disease (18). Single cell sequence data from mouse kidney has more clearly defined cell types than equivalent human data allowing for better assignment of genes to cell types. Thus to identify the particular cell types where our CICs are expressed, We reanalyzed published single cell transcriptomes from healthy mouse kidneys (16) to construct a uniform manifold projection (Fig 3C) where the identities of cell clusters were assigned using consensus marker genes from Chen *et al.* (17) (Fig S3B). The clusters broadly agreed with original cell type assignments by Ransick *et al.* (16) (Fig S3A-C). The three main expression patterns we found include genes restricted to epithelial cells (genes such as Tacstd2, Cdkl1, Akap12, and Aif1L), those with broad expression in many cells (Osbpl9), and those expressed in stromal cells (Endothelium: F2R; T-cell: Bcl11B) (Fig 3D).

When inspecting our CICs expressed in epithelial cells and showing differential expression in human PKD, the tumor associated calcium signal transducer *Tacstd2* stood out. This gene, whose expression was restricted to epithelial cells of the distal tubule (Fig 3D, 3E) was one of the most dysregulated genes in human PKD (FDR $<1E^{-10}$) (Fig3B and Table S3). In our data, Tacstd2 was dysregulated in P6 pre-cystic kidneys, P10 early cystic kidneys, and in early time points of Woo *et al.*'s *Pkd1* AND *Pkd2* models (Fig S2B). In healthy human kidneys most cells show low to undetectable expression, but the expression goes up considerably in the distal parts of the uriniferous tubule in PKD tissues (Fig3F,3G).

Validating Tacstd2 as a cyst initiation candidate

To validate the epithelial expression of *Tacstd2* predicted by single-cell RNAseq, we immuno-stained kidney tissues collected from the same cohort of animals that were used for RNA

isolation in this study (Fig 4A, 4B). In addition, to see how *Tacstd2* responds in more highly cystic kidneys, we examined P21 tissue collected from another study where *Pkd2* was deleted in the early post-natal period by tamoxifen treatment of mothers nursing *Rosa26-Cre^{ERT2}*, *Pkd2$^{flox/flox}$* pups (20) (Fig 4A, 4B). We find that Tacstd2 does not stain proximal tubules in either control or *Pkd2* mutant tissue but does label collecting ducts in both control and experimental kidneys (Fig 4C). While Tacstd2 is found in control collecting ducts, the signal is higher in the experimental collecting ducts at all time points (Fig 4A, B). When normalized by DAPI signal to represent the total number of cells, Tacstd2 is significantly increased in experimental compared to control at P10 and P21. At P6 the difference did not reach significance (Fig 4B). All images used for quantification are included in Fig S4.

The elevated Tacstd2 expression in our *Pkd2* mutant mouse kidneys prompted us to ask whether TACSTD2 expression was also elevated in human ADPKD samples. To do this, we obtained three sections of adult male non-cystic and three sections of male cystic kidneys. The genotypes are unknown, but the early disease development in these patients is suggestive of *PKD1* mutations. Similar to what we observed in our murine models, TACSTD2 is only faintly detected in control tissues but is strongly observed in the cyst-lining epithelial tissue from cystic patients and overall levels of TACSTD2 signal were higher in the cystic kidneys (Fig 5A, 5B).

Since we were unable to determine the genotypes of the patient samples, we wanted to determine whether TACSTD2 is elevated by polycystin loss in human kidney organoids with defined genotypes. To do this, we used control, *PKD1$^{-/-}$*, and *PKD2$^{-/-}$* IPS cells generated by the PKD Research Resource Consortium to generate organoids using a slightly modified Ruiter *et al.* protocol [21]. This protocol produced robust cysts from both mutant lines although the *PKD1$^{-/-}$*-derived organoids were more extensively cystic (Fig 5C). Control organoids showed little staining with TACSTD2 antibodies while *PKD1$^{-/-}$* and *PKD2$^{-/-}$* organoids showed robust TACSTD2 label of the tubules and cysts. The very large cysts that develop when *PKD1$^{-/-}$* is mutated were strongly stained (Fig 5D, 5E). TACSTD2 stained the whole cell with highest concentration at the cell surface (Fig 5D). From this analysis, we conclude that TACSTD2 is increased by loss of either *PKD1* or *PKD2*.

Discussion

Improving ADPKD treatment and outcomes depends on understanding genetic changes that promote cyst development. Focusing on meaningful changes in renal gene expression that precede cyst formation has been challenging due to low amplitude gene expression within low abundance cell types in heterogeneous tissues. Previous investigations (14) found few genes differentially expressed in pre-cystic time points but found many differentially expressed genes later disease stages. However, the genes elevated in grossly cystic tissue generally participate in broad proliferative pathways, and do not inform the mechanisms of cyst initiation.

With these previous studies and pitfalls in mind, we set out to identify potential cyst drivers by controlling the timing of *Pkd2* loss. To find low amplitude changes present before gross cyst formation, we utilized a high number of animals with equal sex parity. We then cross referenced our data to previous studies to find genes with consistent changes. We further cross referenced our differentially expressed genes against human disease and murine single cell atlases to focus on conserved cystogenic changes in epithelial cells. Through our multispecies, multiomic approach, we identified 74 cyst initiation candidates including tumor-associated calcium signal transducer 2 (*Tacstd2*).

While our data agrees overall with Kunnen *et al.* (22), and Zhang *et al.* (23), it is fairly divergent from Woo *et al.* (14). We observed that *Tacstd2* is robustly elevated in the Woo *et al.* data, but not in the Kunnen *et al.* or Zhang *et al.* data. A major difference between the studies is the age at which polycystin is deleted. In both Kunnen *et al.* and Zhang *et al.*, the animals are mature at the time of deletion, while in our study and *Woo et al.'s* the animals lose polycystin in the early postnatal stage when mouse kidneys are still developing. Humans with ADPKD mutations lack polycystin during kidney development *in utero*. It is possible that *Tacstd2/TACSTD2*'s role in cyst initiation may depend on developmental timing. The discrepancies between studies highlight the importance of using an array of genetic models, targets, and time points, to elucidate cyst initiators.

To verify that Tacstd2 is a *bona fide* epithelial cyst initiating candidate we immunostained tissues for Tacstd2. Consistent with our RNAseq study, we found staining slightly elevated in experimental kidneys compared to controls at P6 and dramatically elevated

at P10. Mouse findings were consistent with human kidney tissues and organoids, suggesting that TACSTD2 is a relevant target in human disease.

Tacstd2, also known as trophoblast cell surface antigen 2 (Trop2), is a transmembrane protein originally identified in trophoblast cells (24) and subsequently found to be highly expressed in many solid tumors (25). It appears to be an oncogene as overexpression increases proliferation of cancer cells with low basal expression and knockdown with siRNA reduces growth of cancer cells with high expression (26). Its ability to mark cancer cells has led to the development of antibody drug conjugate therapies to deliver cytotoxic payloads to cancer cells (10). The FDA approved drug, Sacituzumab govitecan (Trodelvy), which is a conjugate to a topoisomerase I inhibitor, is in clinical use to treat metastatic triple-negative breast cancer and advanced or metastatic urothelial carcinoma. Side effects of nausea, fatigue, alopecia, febrile neutropenia, myelosuppression, and diarrhea leading to dehydration and acute kidney injury were observed but other kidney toxicities were not reported. A second drug Datopotamab Deruxtecan is being explored in several clinical trials and has shown reduced side effects. Kidney effects were not reported (27). To the best of our knowledge Tacstd2 expression has not previously been explored in relation to ADPKD. While antibody drug conjugates to topoisomerase inhibitors may be too toxic for long term use in PKD patients, adapting the conjugates to carry anti-cyst payloads such as rapamycin could increase the efficacy of an anti-cyst drug while reducing its off-target effects.

Two mouse *Tacstd2* mutant lines have been generated. Contrary to expectations, the mice were viable and in the first report, no pathology was observed (28). The second line generated by KOMP shows microphthalmia and small testis but no other phenotypes (https://www.mousephenotype.org/data/genes/MGI:1861606). Humans with pathological variants in *TACSTD2* develop gelatinous drop-like corneal dystrophy, which is a degenerative disease of the cornea (29). In the cornea, TACSTD2 is thought to bind to claudins 1 and 7 to maintain the structure of the tight junctions. When TACSTD2 is defective, the cornea becomes more permeable and accumulates amyloid, ultimately leading to vision loss (30). The relatively mild phenotypes of mouse and humans lacking TACSTD2, supports the idea that this gene product could be targeted without causing major off target effects.

In the context of PKD, it is interesting to note that antibodies binding the extracellular domain of Tacstd2 transiently increase cytoplasmic calcium concentration, possibly from an intracellular store (31). The cytoplasmic tail of Tacstd2 contains a PIP_2 binding site and numerous pathways are affected by Tacstd2. In tumor cells, AKT signaling shows strong correlation with Tacstd2 expression (32) but MAPK/ERK, ErbB, TGFβ, Wnt/β-catenin, JAK/STAT, and integrin signaling have all been implicated as downstream targets of Tacstd2 (33). Wnt/β-catenin signaling is particularly interesting as this pathway is disturbed in PKD. β-catenin binds directly to Tacstd2 and Tacstd2 over expression promoted nuclear accumulation of β-catenin (34). This observation could have implications for driving cyst formation in PKD as expression of activated β-catenin is sufficient to drive cyst formation (35).

In conclusion, our work demonstrates that Tacstd2 is elevated early in cystic kidney tissue as well as human polycystic kidneys. The insights gained from studies of breast and other aggressive cancers suggest that Tacstd2 is a promoter of cell proliferation and could play a key role in cyst formation. Further studies are needed to elucidate the mechanistic role of Tacstd2 in PKD. Our work suggests that Tacstd2 is a promising target in PKD and should be explored as a therapeutic target. More immediately, our work indicates that patients with PKD who receive anti-TACSTD2 therapy should be monitored for kidney effects.

Experimental Procedures

Mouse studies

Mouse strains used include *Pkd2*^{flox} (11), *Cagg-Cre*^{ER} (36), and *Rosa26-Cre*^{ERT2} (37). *Pkd2*^{flox} was converted to *Pkd2*^{null} by crossing to the germline *Stra8-Cre* (38) to delete the floxed exons. All mice were C57BL/6J congenics maintained by backcrossing to C57BL/6J purchased from Jackson Laboratory (Bar Harbor Maine, USA). These studies were approved by the Institutional Animal Care and Use Committee of the University of Massachusetts Chan Medical School.

For RNA sequencing, pups segregating *Pkd2*$^{+/flox/null}$ and *Cagg-Cre*^{ER} were dosed with tamoxifen (50 mg/kg) by intraperitoneal injection on postnatal day 2 (P2). On postnatal day 6 (P6) or day 10 (P10), paired kidneys were immediately frozen in RNA later, and total RNA was isolated as previously described (39) (Fig 1A).

For histology of P21 kidneys (Fig 4 only), mothers were dosed with tamoxifen (200 mg/kg) by oral gavage on P2, 3, and 4. The *Pkd2*$^{flox/flox}$*, Rosa26-Cre*^{ERT} pups remained with nursing mothers until euthanasia at P21 as previously described (20).

RNA sequencing

mRNA

Libraries were prepared for 100bp paired-end sequencing by BGI Genomics (Yantian District, Shenzhen, China). Read quality assessment, alignment and counting were performed using DolphinNext pipeline (40). The modules used were FastQC v0.11.7 (https://www.bioinformatics.babraham.ac.uk/projects/fastqc/) and kallisto v0.46.1 (41). Differential expression analysis was performed using DESeq2 (42). Very low expression genes were excluded using cutoff counts per million (CPM) <2 in at least 48 samples. Inclusion criteria for significant differentially expressed genes (DEGs) consisted of FDR < 0.05.

Small RNA

Small RNA libraries were prepared for 50bp single-end sequencing by BGI Genomics (Yantian District, Shenzhen, China). The sequences were demultiplexed and underwent bar code and adapter sequence removal using the SOAPnuke software (43). The steps for demultiplexing, bar code removal and adapter removal were carried out by BGI. Read quality assessment, alignment and miRNA prediction and quantification/gene expression calculation as well as differential expression were performed using the Omiras pipeline (44) which uses Bowtie for read mapping (45), mirDeep2 for finding novel miRNA (46), and DESeq for normalizing the data and calculating differential expression (47). Inclusion criteria for significant differentially expressed microRNAs (DEmirs) consisted of raw read counts > 0, FDR < 0.05, and identified as mature or stem-loop microRNAs.

Comparison to published bulk RNAseq data

Comparisons to published mouse datasets were performed by filtering publicly available data for genes with FDR <0.05 and comparing them against genes in our dataset with FDR <0.05. Simple linear regression analysis was performed using GraphPad Prism 9, Version 9.5.1. Datasets include:

- (22) Supplementary Table S9. Fold change of differentially expressed genes in mice deleted of *Pkd1* by KspCad-Cre^{ERT2} compared to *Pkd1* wild type controls.
- (14) Supplementary Table S1. Differentially expressed genes in mice deleted of *Pkd1* by HoxB7-Cre.
- (14) Supplementary Table S3. Differentially expressed genes in mice deleted of *Pkd2* by HoxB7-Cre.
- (23) Supplementary Data 2. Differentially expressed genes in mice deleted of *Pkd2* by Pax8^{rtTA},TetO-Cre.

Comparison to published single-cell RNAseq analysis

Gene Expression Omnibus (GEO) murine

Our present work examines changes in whole-kidney gene expression following *Pkd2* deletion but does not identify which of the diverse renal cell types express the gene. To determine whether there is any cell-specific localization of candidate genes, we reanalyzed data from Ransick et al. (16), who identified enriched transcriptome profiles within individual renal cell types. Murine transcriptomes were obtained as 12 objects from GSE129798 (16). Raw data was filtered to retain cells that expressed between 200 and 6,000 unique genes and a mitochondrial fraction less than 10%. 31056 cells from the cortex, outer medulla, and inner medulla fit these criteria. Each dataset was further pre-processed by log normalizing each dataset with a scale factor of 10,000 and finding 2,000 variable features using the default 'vst' method in seurat3.0 (48). The dataset was then scaled to regress out differences driven by unequal total counts captured and mitochondrial capture. The top 40 principal components were used for construction of a Uniform Manifold Approximation and Projection (UMAP) and for neighbor finding. During clustering we utilized a resolution parameter of 0.5. The resulting 28 Louvain clusters were visualized in 2D and/or 3D space and were annotated using known biological cell-type markers (17).

GEO wild-type and ADPKD human

To determine if candidate cyst initiation genes from our mouse *Pkd2* model were also expressed in human kidneys, we reanalyzed published renal transcriptome data from human

PKD patients and from healthy controls. Data were obtained as 13 objects from GSE185948 (15).

The data was filtered to only retain cells that expressed between 500 and 6,000 unique genes and a mitochondrial fraction less than 10%. Heterotypic doublets were identified with DoubetFinder v2 assuming 8% of cells represented heterogtypic doubets. The datasets were then integrated in Seruat using "IntegrateData". These parameters resulted in retention of 56,161 cells from the healthy controls and 69,385 cells from PKD patients. Each dataset was further pre-processed by log normalizing each dataset with a scale factor of 10,000 and finding 2,000 variable features using the default 'vst' method in seurat3.0 (48). The top 50 principal components were used for initial integration. The dataset was then scaled to regress out differences driven by unequal total counts captured and mitochondrial capture. The ADPKD and Healthy control datasets were then integrated with batch effect correction using Harmonyv1. The top 15 principal components were used for construction of a UMAP and for neighbor finding. During clustering we utilized a resolution parameter of 0.5. The resulting Louvain clusters were visualized in 2D and/or 3D space and were annotated using known biological cell-type markers (17).

For pseudobulk analysis cells were grouped by their disease state, and the Seurat function "AverageExpression" was used to average expression across all cell types present in each sample. This data was then rescaled and visualized in heatmaps. Differentially expressed genes between the ADPKD and healthy controls were calculated using "FindMarkers" filtering for transcripts with a log2FC greater than 0.25 and expression in greater than 20% of cells.

Kidney organoid differentiation

Human induced pluripotent stem (IPS) cells were obtained from PKD Research Resource Consortium University of Maryland (Baltimore, Maryland) and verified to be of human origin and to have the correct genotype by sequencing of the regions of *PKD1* and *PKD2* targeted by the guides.

To produce organoids, on day 0, IPS cells were plated at 7,300 cells per cm^2 in mTeSR™1 media (Stemcell 85850, Kent, WA) on vitronectin (ThermoFisher Scientific A14700, Carlsbad CA) coated 6-well plates. On day 1, differentiation was initiated by replacing medium with STEMdiff

APEL2 Medium (Stemcell 05275, Kent, WA) containing 8µM CHIR99021 (Abcam ab120890, Cambridge, MA) for four days. The media was replaced with fresh media every two days. On day 5, cells were washed with Gibco DPBS, no calcium, no magnesium (ThermoFisher Scientific), and media replaced with fresh APEL2 media containing 50ng/mL of recombinant human FGF9/GAF protein (Abcam ab50034) and 1µg/ml of 0.2% heparin sodium salt in dissolved in PBS (Stemcell 07980, Kent, WA) for three days. On day 7, the media was replaced with APEL2 containing 5µM CHIR99021 for 1 hr. Cells were then washed and dislodged using TrypLE Express without phenol red (Thermo-Fisher 12604013) and then spun down. The cells were then resuspended in APEL2 containing FGF9 50ng/mL and Heparin 1µg/mL, transferred to an Ultra-Low Attachment Multiple Well Plate (Costar size 6 well, flat bottom CLS3471, Allentown, PA) and placed on an orbital shaker at 100 rpm in 37˚C 5% CO_2 incubator. Media was changed every two days. After five days, the medium was replaced with APEL2 without additions and changed every two days. Organoids were typically harvested 14 days later. This protocol is a modification of Ruiter et. al[21].

Histology

Mouse tissues

Tissues were fixed by immersion overnight in 10% formalin (Electron Microscopy Sciences) in phosphate-buffered saline and then embedded in paraffin. Sections were deparaffinized and stained with hematoxylin and eosin (H&E).

Images of H&E-stained sections were obtained with a Zeiss Axio Scan.Z1 slide scanner with brightfield capabilities using the 20X objective.

For immunofluorescent staining, sections were deparaffinized, antigens were retrieved by autoclaving for 30 min in 10 mM sodium citrate, pH 6.0 and stained with primary antibodies diluted in TBST (10 mM Tris, pH 7.5, 167 mM NaCl, and 0.05% Tween 20) plus 0.1% cold water fish skin gelatin (Sigma-Aldrich). Alexa Fluor–labeled secondary antibodies (Invitrogen) were used to detect the primary antibodies. Primary antibodies used included Aquaporin-2 (1:200; Sigma #SAB5200110), Tacstd2/Trop-2 (F-5) (1:250, Santa Cruz #sc-376181). FITC-conjugated lectins were added with secondary antibodies: Lotus tetragonolobus agglutinin (LTA, 1:50,

Vector Labs) or Dolichos biflorus agglutinin (DBA, 1:20, Vector Labs). Nuclei were labeled with 4',6-diamidino-2-phenylindole (DAPI).

Fluorescent images were obtained with a Zeiss LSM900+ Airyscan microscope. Fluorescent slide scans were obtained using Zeiss Axio Scan.Z1 slide scanner at 20X objective.

Human tissues

Paraffin slides of kidney sections from 3 male ADPKD samples and 3 healthy male controls were obtained from the Polycystic Kidney Disease Research Resource Consortium at the University of Maryland (Baltimore, Maryland). No genotype or additional information is available for these specimens. Slides were deparaffinized, antigens retrieved, and stained as described above using Aquaporin-2 (1:200; Sigma #SAB5200110), Tacstd2/Trop-2 (F-5) (1:250, Santa Cruz #sc-376181), FITC-conjugated Lotus tetragonolobus agglutinin (LTA, 1:50, Vector Labs).

Fluorescent images were obtained with a Zeiss LSM900+ Airyscan microscope. Fluorescent slide scans were obtained using Zeiss Axio Scan.Z1 slide scanner at 20X objective.

Organoids

Plates were tilted until kidney organoids settled to the bottom and medium was slowly removed with a 5ml pipette. Organoids were washed with 2 ml of PBS and again allowed to settle to the bottom of the dish. After removal of the PBS, 2ml of 4% paraformaldehyde in PBS was added for 1 hr. Following this, paraformaldehyde was removed and organoids were resuspended in 500 µL of PBS in a microcentrifuge tube. The PBS was replaced with 200 µL of 30% sucrose in 100mM Sorensen's Phosphate Buffer. After 24 hrs, the organoids were transferred to a cryomold and embedded in Tissue Plus O.C.T. Compound (Fisher HealthCare 4585). Embedded organoids were frozen on dry ice. Cryoblocks were sectioned at 10 microns and collected on Superfrost Plus Microscope slides (Fisherbrand 12-550-150).

Slides were washed with PBS containing 0.1% Tween20 (PBS-T) at 37°C for 10 min. The organoids fragments on the slide were circled with SuperHT Pap Pen (Biotium 22006, Fremont, CA). 300 µL of blocking solution (5% donkey serum in PBS-T) was applied to each slide and incubated at room temperature in a humidified chamber for 1 hr. After removal of the blocking solution, primary antibodies diluted in 5% BSA in PBS-T were incubated overnight at room temperature in a humidified chamber. After three washes, secondary antibodies diluted in 5%

BSA in PBS-T were added for 2 hrs in the dark. Then slides were washed three times with PBS-T for 30 min. Slides were air-dried for 5 min and coverslips were mounted with Prolong™ Gold Antifade Mountant with DAPI (Invitrogen by Thermo Fisher Scientific P36935).

Fluorescent images were obtained using a ZEISS LSM900+ Airyscan microscope and analyzed by ZEN lite software.

Supplemental Material Table of Contents

Supplemental Table 1: Differentially expressed genes at P6.

Supplemental Table 2: Differentially expressed genes at P10.

Supplemental Table 3: Overlap of Differentially expressed genes at P10 and ADPKD.

Supplemental Figure 1: Small RNAseq of Pkd2 experimental kidneys vs control at P10 identifies microRNAs with known association in PKD.

Supplemental Figure 2: Differentially expressed mRNAs in pre-cystic and early cystic mouse kidneys.

Supplemental Figure 3: *Tacstd2* expression in cystic epithelium.

Supplemental Figure 4: Tacstd2 expression in cystic mouse renal epithelium.

Figures and Figure Legends

Figure 1

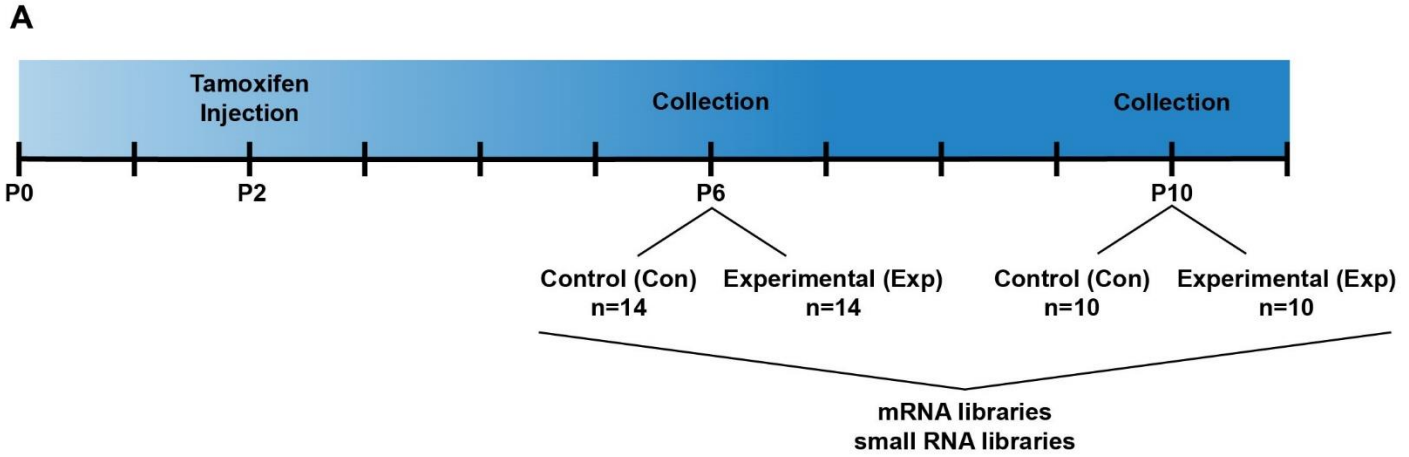

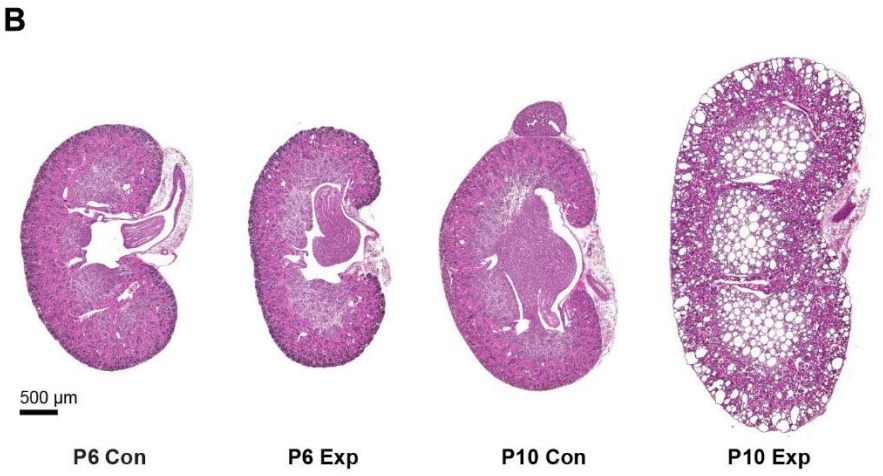

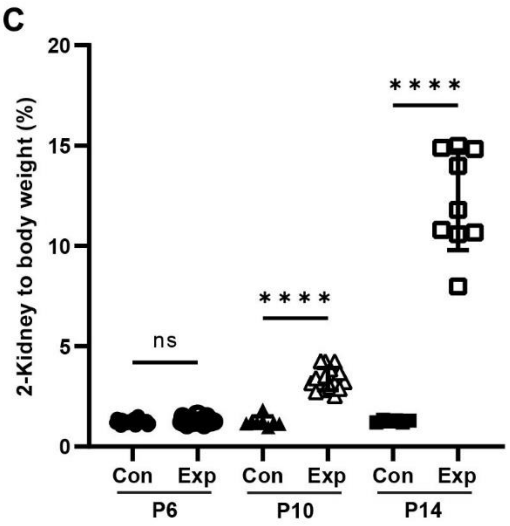

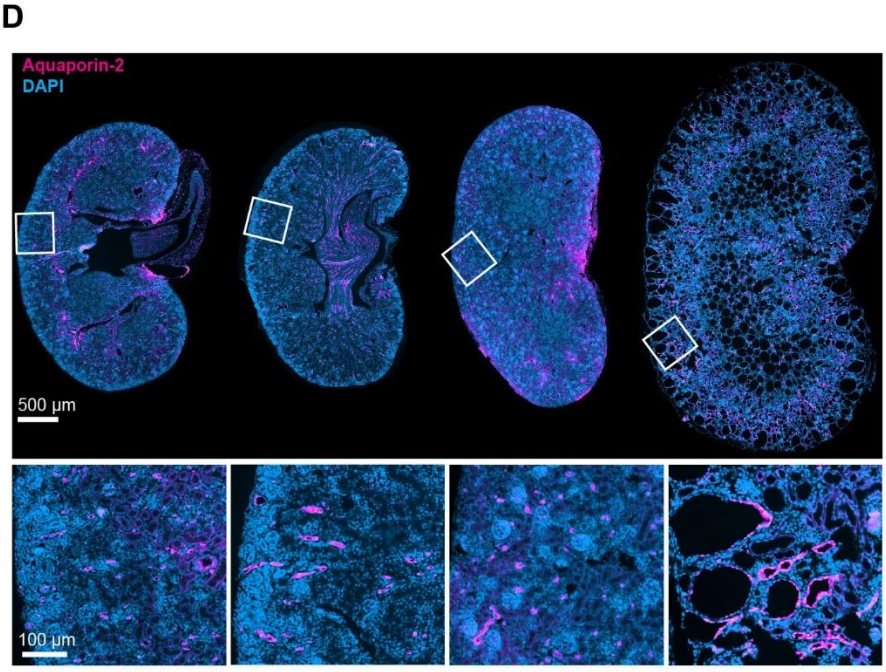

Figure 1. *Pkd2* deletion at postnatal day 2 (P2) induces rapid cyst growth.

Mouse genotypes: Con (*Cagg-Cre^{ER}, Pkd2$^{flox/+}$* or Cre-negative, *Pkd2$^{flox/null}$*), Exp (*Cagg-Cre^{ER}, Pkd2$^{flox/null}$*).

(A) Tamoxifen induction occurred at P2 followed by kidney collection for RNA sequencing at P6 and P10. Parallel mRNA and small RNA libraries were prepared.

(B) H&E staining show the extent of disrupted organ architecture. Images captured by Zeiss Axio Scan.Z1 with 20X objective. Scale bar is 500 microns and applies to all images in the panel.

(C) Cystic burden was quantified using the ratio of 2-kidney weight / body weight x 100%. N is 28 (P6 Con), 27 (P6 Exp), 8 (P10 Con), 16 (P10 Exp), 6 (P14 Con), 9 (P14 Exp). ****, $p < 0.0001$; ns, not significant by one-way ANOVA followed by Tukey multiple comparison test with multiplicity-adjusted p-values. Error bars indicate SD.

(D) Kidney sections were probed for collecting duct marker Aquaporin-2 (red). Nuclei were marked by DAPI. Images captured by Zeiss Axio Scan.Z1 with 20X objective. Insets from indicated regions show detail of collecting duct at higher power. Scale bar is 500 microns for full size images, 100 microns for enlargements.

Figure 2

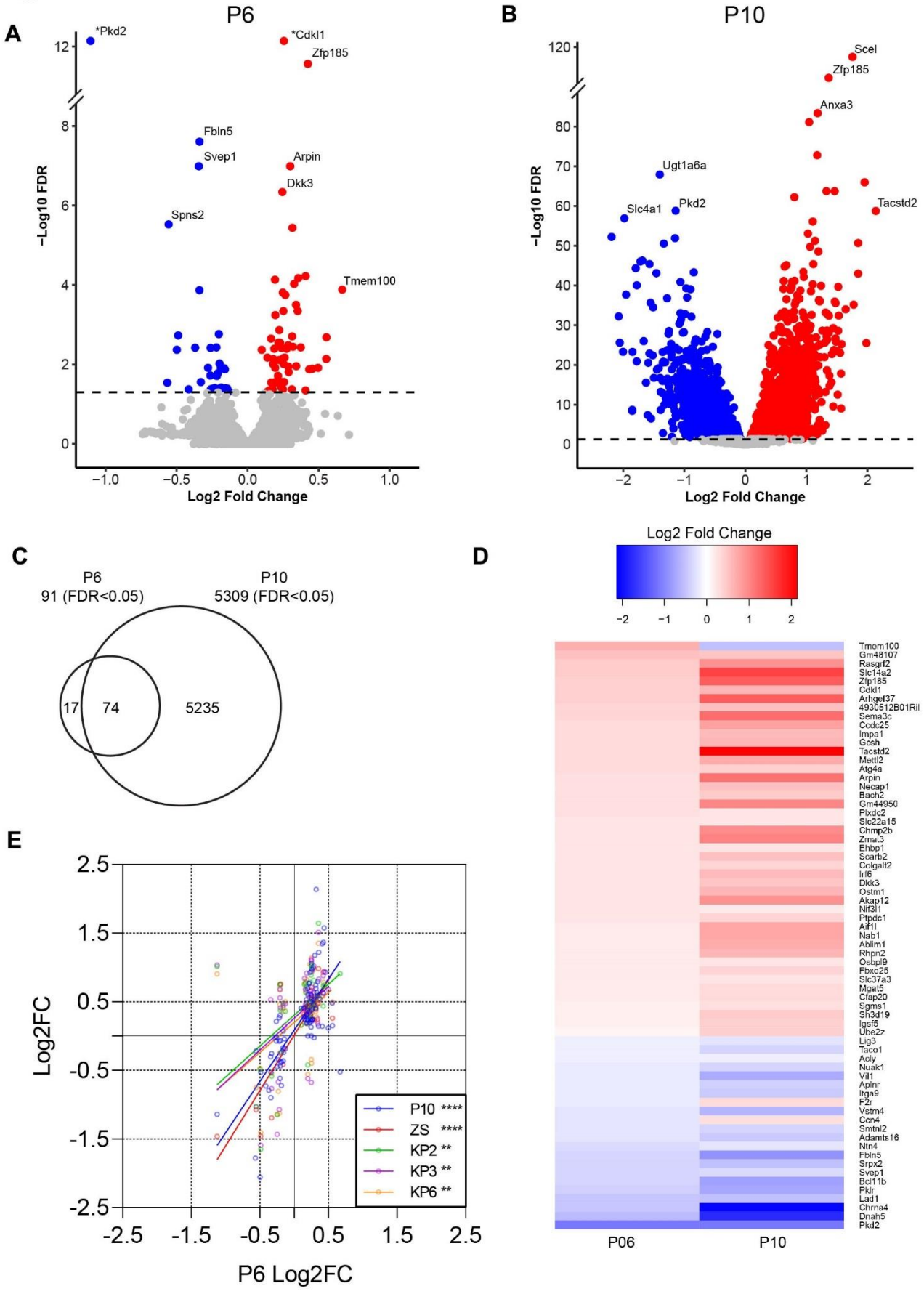

Figure 2. Identifying cyst initiation candidate genes through mRNA sequencing *Pkd2* mouse kidneys at pre-cystic and early cystic time points.

(A) Volcano plot showing pre-cystic (P6) differentially expressed genes (DEGs; DESeq2). Colored dots indicate FDR <0.05, red indicates increased and blue decreased in Experimental vs Control. Plot was cropped for better visualization. (*) Data point moved for better visualization: Pkd2 [Log2(FC) = -1.13, -Log10(FDR) = 93.97], Cdkl1 [Log2(FC) = 0.42, -Log10(FDR) = 26.30].

(B) Volcano plot showing early cystic (P10) DEGs (DESeq2). Colored dots indicate FDR <0.05, red indicates increased expression and blue decreased expression in Experimental vs Control.

(C) The intersection between P6 DEGs (91) and P10 DEGs (5,309) includes 74 genes which we defined as cyst initiation candidates (CICs).

(D) Heatmap showing the relative expression of all CICs at P6(left) and P10 (right),

(E) Scatter plot showing correlation of CICs with published data sets. P6 DEG expression (Log2FC) represented along x-axis vs. P10 and published datasets on y-axis (Log2FC). Datasets include ZS (*Pkd2*) (23) and KP2/3/6 (*Pkd1*; 2 weeks, 3 weeks and 6 weeks post-induction respectively) (22). Details of each study can be found in Table 2. There is significant correlation between P6 and each group by simple linear regression analysis (two-tailed p-values: P10, p<0.0001; ZS, p<0.0001; KP2, p=0.0014; KP3, p=0.0016; KP6, p=0.0012).

Figure 3

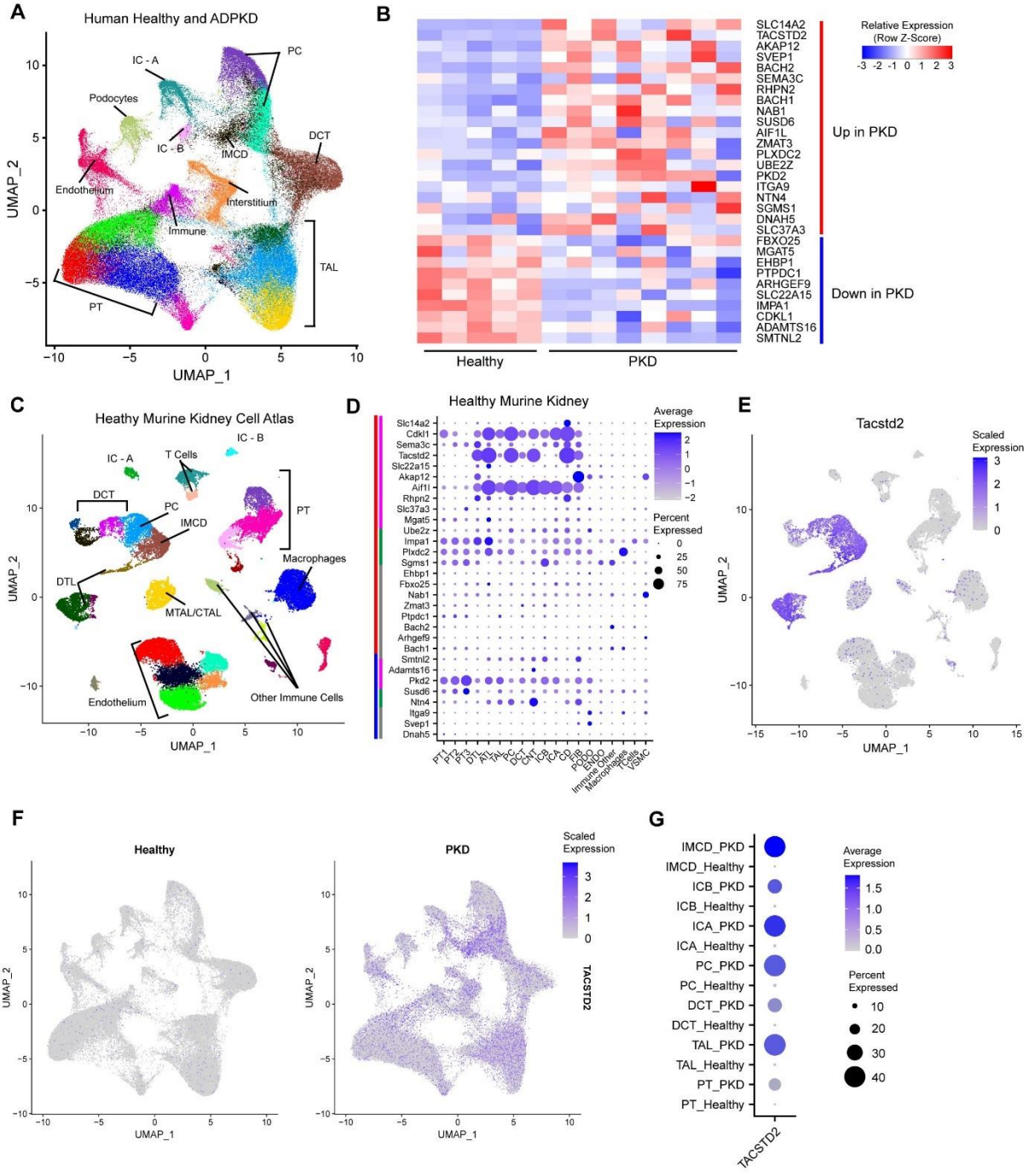

Figure 3. Leveraging multispecies single cell RNAseq to identify tubular cystogenic targets.

(A) UMAP visualization of human kidney cells from healthy and ADPKD tissue (15). DCT: Distal Convoluted Tubule, PT: Proximal Tubule, IC-A: Intercalated Cell – A, IC-B: Intercalated Cell – B, PC: Principal Cell, IMCD: Inner Medullary Collecting Duct, DTL: Descending Thin Limb of Henle, ATL: Ascending Thin Limb of Henle, MTAL/CTAL: Medullary Thick Ascending Limb of Henle/Cortical Thick Ascending Limb of Henle.

(B) Pseudobulk heatmap showing expression of candidate genes (based on murine data in Fig 2) in healthy (n=5) vs ADPKD (n=8) human kidney tissue (15). The candidates shown are differentially expressed using the Wilcox sum in "FindMarkers" and ordered by log2FC. FDR < 0.01. Red bar signifies up in human ADPKD kidney vs healthy control kidney. Blue bar signifies down in human ADPKD vs healthy control kidney. Row-normalized expression.

(C) UMAP visualization of murine kidney cells from Ransick et al.'s Kidney Cell Atlas (16). DCT: Distal Convoluted Tubule, PT: Proximal Tubule, IC-A: Intercalated Cell – A, IC-B: Intercalated Cell – B, PC: Principal Cell, IMCD: Inner Medullary Collecting Duct, DTL: Descending Thin Limb of Henle, ATL: Ascending Thin Limb of Henle, MTAL/CTAL: Medullary Thick Ascending Limb of Henle/Cortical Thick Ascending Limb of Henle.

(D) DotPlot visualizing the localization of conserved murine/human differentially expressed CICs to cell types found in the murine kidney cell atlas. Dot radius represents the percentage of cells in cluster expressing the gene. Opacity scale indicates average gene expression level within expressing cells. Row normalized. Main bars (far left) represent increased expression (red) or decreased expression (blue) in our data; sub bars (left) represent epithelial restricted expression (magenta), broad expression (green), and stromal/indeterminate (gray). Black arrow points to *Tacstd2*, an epithelial cyst initiating candidate.

(E) Feature plot highlighting the expression profile for *Tacstd2* in healthy mouse kidney.

(F) Feature plot highlighting the diffusely increased expression profile for *TACSTD2* in ADPKD vs healthy human kidneys.

(G) DotPlot comparing *TACSTD2* expression in human healthy and ADPKD kidneys as seen in C by cell type labeled in A (15).

(C) UMAP visualization of murine kidney cells from Ransick et al.'s Kidney Cell Atlas (16). DCT: Distal Convoluted Tubule, PT: Proximal Tubule, IC-A: Intercalated Cell – A, IC-B: Intercalated Cell – B, PC: Principal Cell, IMCD: Inner Medullary Collecting Duct, DTL: Descending Thin Limb of Henle, ATL: Ascending Thin Limb of Henle, MTAL/CTAL: Medullary Thick Ascending Limb of Henle/Cortical Thick Ascending Limb of Henle.

Figure 4

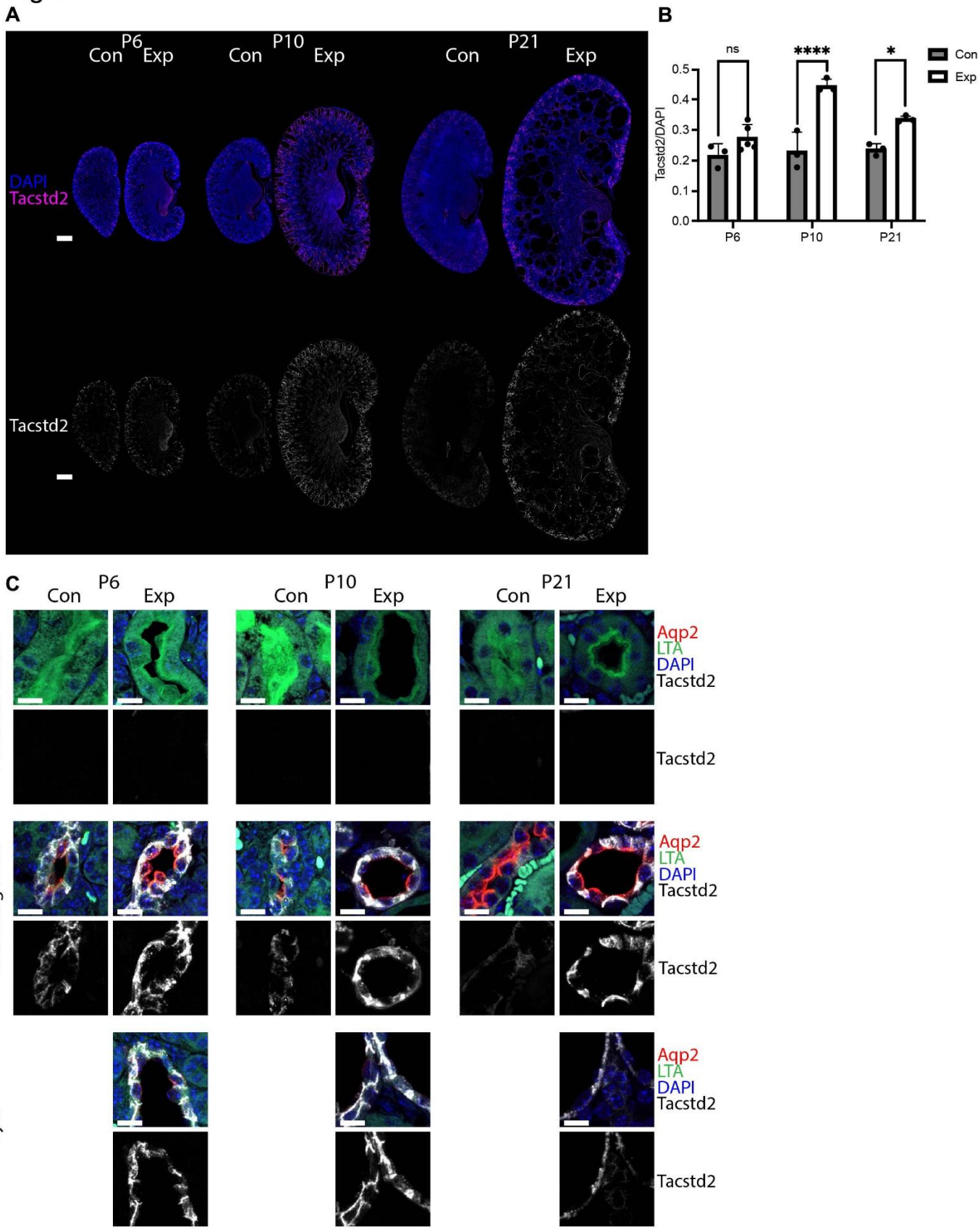

Figure 4. Validating *Tacstd2* expression in mouse kidney epithelium.

(A) Mouse kidney sections were probed for Tacstd2 (fuchsia) and DNA (DAPI, blue). Bottom row shows only the Tacstd2 channel in grey scale. Slide scans were captured by Zeiss Axio Scan.Z1 with 20X objective. Scale bars 500 microns.

(B) Mean intensity of Tacstd2 fluorescence was measured for Control (Con) and Experimental (Exp) mouse kidneys from three age groups: P6, P10 and P21. Normalized by mean intensity of DAPI. P10, P21 and P6 WT (n=3); P6 KO (n=5). Mixed effects analysis with multiple comparisons was performed. Factors included age ($p=0.0019$) and genotype ($p<0.0001$). Non-significant, ns; *, $p<0.05$; ****, $p<0.0001$).

(C) Tissues described in (A) and (B) were imaged using AiryScan LSM 900 with 63X objective. Maximum intensity projections of a 5-micron section imaged at 0.3 micron intervals. Tissue was stained for the collecting duct marker aquaporin2 (Aqp2, red), proximal tubule marker *Lotus tetragonolobus* Agglutinin (LTA, green), nuclei (DAPI, blue) and Tacstd2 (white). Bottom row of each pair shows the Tacstd2 channel in grey scale. Scale bars 10 microns.

Figure 5

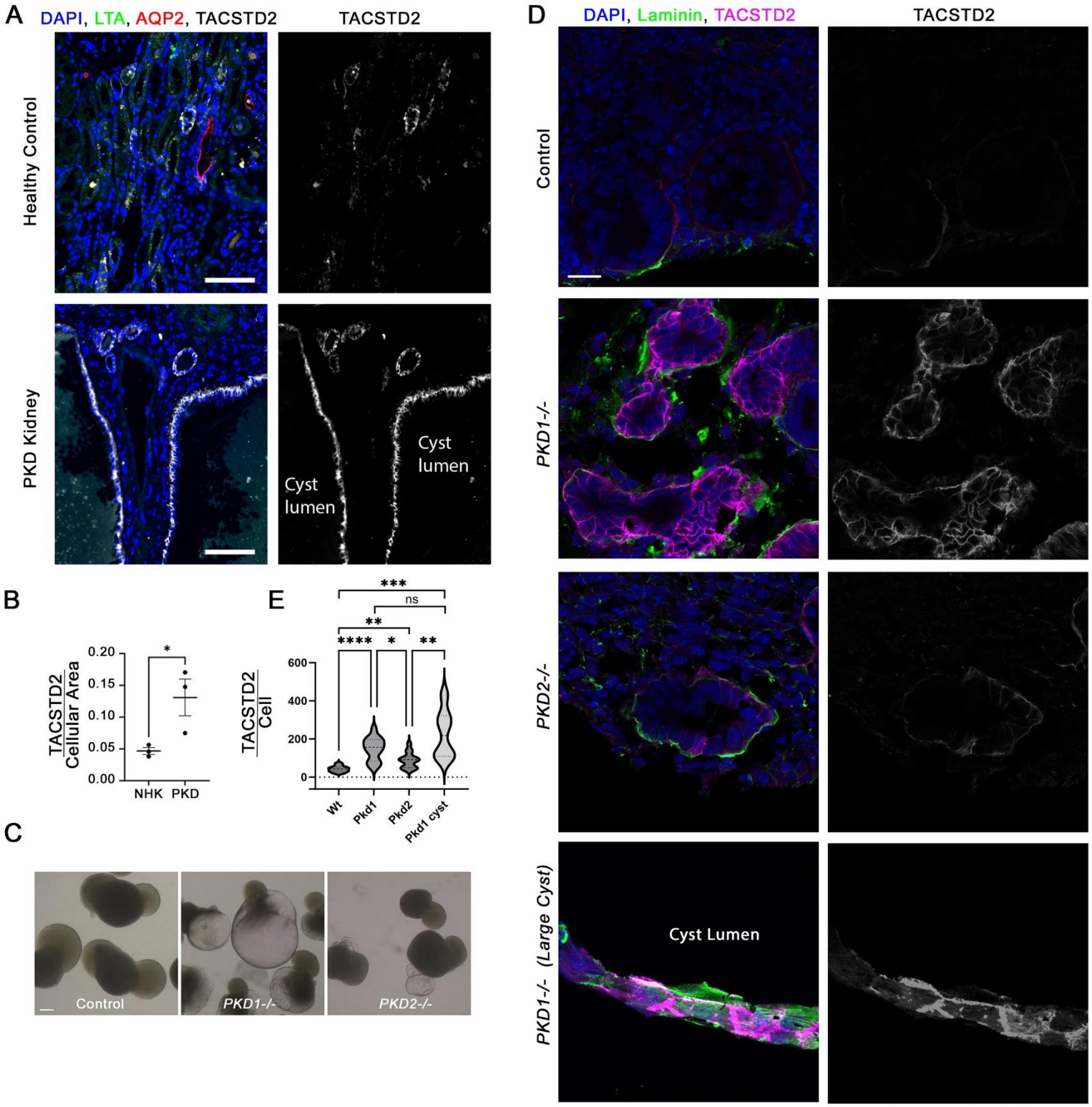

Figure 5. Validating *TACSTD2* expression in human kidney epithelium.

(A) Healthy and ADPKD human kidney sections were probed for TACSTD2 (white), collecting duct marker Aquaporin-2 (AQP2, red) and proximal tubule marker Lotus tetragonolobus Agglutinin (LTA, green). Nuclei were marked by DAPI (blue). The Tacstd2 channel is shown in grey scale in the right image of each pair. Images captured by Zeiss AxioScan.Z1 with 20x objective. Scale bar is 100 microns.

(B) Mean intensity of TACSTD2 fluorescence was measured for normal healthy kidney (NHK) and ADPKD human kidney samples normalized by cellular area. NHK n=3; ADPKD n=3. Unpaired t-test was performed. * p=0.045.

(C) Brightfield images of organoids derived from control, *PKD1*$^{-/-}$, and *PKD2*$^{-/-}$ mutant cells. Scale bar is 200 microns.

(D) Immunofluorescence of organoid sections stained for TACSTD2 (fuchsia or white), laminin (green) and DAPI (blue). Scale bar is 20 microns.

(E) Quantification of the images shown in D. Significance as compared to control *p<0.05; **p<0.01 ; ***p<0.001 ; ****p<0.0001; ns not significant by Welch and Brown-Forsythe ANOVA.

Table 1. Experimental design

Timepoints	**PKD2 Control (Con)** *Cagg-Cre^{ER},Pkd2$^{+/flox}$* (n=20) or *Pkd2$^{null/flox}$*, [no Cre] (n=4)	**PKD2 Deletion (Exp)** *Cagg-Cre^{ER}, Pkd2$^{null/flox}$* (n=24)
P6 (n=28)	Male (n=7) Female (n=7) Total (n=14)	Male (n=7) Female (n=7) Total (n=14)
P10 (n=20)	Male (n=3) Female (n=7) Total (n=10)	Male (n=5) Female (n=5) Total (n=10)

Table 2. Early and pre-cystic mouse models with RNAseq data

Publication	Cre	Target Gene	Induction conditions	Age at sacrifice	Degree of Cysts
This Work	*Cagg-Cre^{ER}* – whole body	*Pkd2*	Tamoxifen IP at P2	P6	Pre
"	*Cagg-Cre^{ER}* – whole body	*Pkd2*	Tamoxifen IP at P2	P10	Early
Kunnen *et al.*(22)	*KspCad-Cre^{ERT2}* – kidney specific	*Pkd1*	Tamoxifen in food 5mg/day x 3 days at 13-14 weeks of age	13/14 + 2 weeks	Pre
"	*KspCad-Cre^{ERT2}* – kidney specific	*Pkd1*	Tamoxifen in food 5mg/day x 3 days at 13-14 weeks of age	13/14 + 3 weeks	Pre
"	*KspCad-Cre^{ERT2}* – kidney specific	*Pkd1*	Tamoxifen in food 5mg/day x 3 days at 13-14 weeks of age	13/14 + 6 weeks	Pre
Zhang *et al.* (23)	Pax8^{rtTA},TetO-Cre – kidney selective, whole nephron	*Pkd2*	Doxycycline in drinking water + sucrose 2mg/mL for 2 weeks starting at P28-P42	P70	Pre
Woo *et al.* (14)	*HoxB7-Cre* – collecting duct	*Pkd2*	*HoxB7-Cre* becomes active E9.5-E12.5	P1	Pre
"	*HoxB7-Cre* – collecting duct	*Pkd2*	*HoxB7-Cre* becomes active E9.5-E12.5	P3	Early
"	*HoxB7-Cre* – collecting duct	*Pkd2*	*HoxB7-Cre* becomes active E9.5-E12.5	P7	Mid
"	*HoxB7-Cre* – collecting duct	*Pkd1*	*HoxB7-Cre* becomes active E9.5-E12.5	P1	Pre
"	*HoxB7-Cre* – collecting duct	*Pkd1*	*HoxB7-Cre* becomes active E9.5-E12.5	P3	Early
"	*HoxB7-Cre* – collecting duct	*Pkd1*	*HoxB7-Cre* becomes active E9.5-E12.5	P7	Mid

References

1. Lanktree, M. B., Haghighi, A., Guiard, E., Iliuta, I. A., Song, X., Harris, P. C., Paterson, A. D., and Pei, Y. (2018) Prevalence Estimates of Polycystic Kidney and Liver Disease by Population Sequencing. *J Am Soc Nephrol* **29**, 2593-2600
2. Iglesias, C. G., Torres, V. E., Offord, K. P., Holley, K. E., Beard, C. M., and Kurland, L. T. (1983) Epidemiology of adult polycystic kidney disease, Olmsted County, Minnesota: 1935-1980. *Am J Kidney Dis* **2**, 630-639
3. Dalgaard, O. Z. (1957) Bilateral polycystic disease of the kidneys; a follow-up of 284 patients and their families. *Dan Med Bull* **4**, 128-133
4. Torres, V. E., Chapman, A. B., Devuyst, O., Gansevoort, R. T., Grantham, J. J., Higashihara, E., Perrone, R. D., Krasa, H. B., Ouyang, J., Czerwiec, F. S., and Investigators, T. T. (2012) Tolvaptan in patients with autosomal dominant polycystic kidney disease. *N Engl J Med* **367**, 2407-2418
5. Torres, V. E., Devuyst, O., Chapman, A. B., Gansevoort, R. T., Perrone, R. D., Ouyang, J., Blais, J. D., Czerwiec, F. S., Sergeyeva, O., and Investigators, R. T. (2017) Rationale and Design of a Clinical Trial Investigating Tolvaptan Safety and Efficacy in Autosomal Dominant Polycystic Kidney Disease. *Am J Nephrol* **45**, 257-266
6. McEwan, P., Bennett Wilton, H., Ong, A. C. M., Orskov, B., Sandford, R., Scolari, F., Cabrera, M. V., Walz, G., O'Reilly, K., and Robinson, P. (2018) A model to predict disease progression in patients with autosomal dominant polycystic kidney disease (ADPKD): the ADPKD Outcomes Model. *BMC Nephrol* **19**, 37
7. Cornec-Le Gall, E., Alam, A., and Perrone, R. D. (2019) Autosomal dominant polycystic kidney disease. *Lancet* **393**, 919-935
8. Oberdhan, D., Schaefer, F., Cole, J. C., Palsgrove, A. C., Dandurand, A., and Guay-Woodford, L. (2022) Polycystic Kidney Disease-Related Disease Burden in Adolescents With Autosomal Dominant Polycystic Kidney Disease: An International Qualitative Study. *Kidney Med* **4**, 100415
9. Fick-Brosnahan, G. M., Tran, Z. V., Johnson, A. M., Strain, J. D., and Gabow, P. A. (2001) Progression of autosomal-dominant polycystic kidney disease in children. *Kidney Int* **59**, 1654-1662
10. Bardia, A., Hurvitz, S. A., Tolaney, S. M., Loirat, D., Punie, K., Oliveira, M., Brufsky, A., Sardesai, S. D., Kalinsky, K., Zelnak, A. B., Weaver, R., Traina, T., Dalenc, F., Aftimos, P., Lynce, F., Diab, S., Cortes, J., O'Shaughnessy, J., Dieras, V., Ferrario, C., Schmid, P., Carey, L. A., Gianni, L., Piccart, M. J., Loibl, S., Goldenberg, D. M., Hong, Q., Olivo, M. S., Itri, L. M., Rugo, H. S., and Investigators, A. C. T. (2021) Sacituzumab Govitecan in Metastatic Triple-Negative Breast Cancer. *N Engl J Med* **384**, 1529-1541
11. Garcia-Gonzalez, M. A., Outeda, P., Zhou, Q., Zhou, F., Menezes, L. F., Qian, F., Huso, D. L., Germino, G. G., Piontek, K. B., and Watnick, T. (2010) Pkd1 and Pkd2 are required for normal placental development. *PLoS One* **5**
12. Song, G., Zhang, H., Chen, C., Gong, L., Chen, B., Zhao, S., Shi, J., Xu, J., and Ye, Z. (2017) miR-551b regulates epithelial-mesenchymal transition and metastasis of gastric cancer by inhibiting ERBB4 expression. *Oncotarget* **8**, 45725-45735

13. Wei, Z., Liu, Y., Wang, Y., Zhang, Y., Luo, Q., Man, X., Wei, F., and Yu, X. (2016) Downregulation of Foxo3 and TRIM31 by miR-551b in side population promotes cell proliferation, invasion, and drug resistance of ovarian cancer. *Med Oncol* **33**, 126
14. Woo, Y. M., Kim, D. Y., Koo, N. J., Kim, Y. M., Lee, S., Ko, J. Y., Shin, Y., Kim, B. H., Mun, H., Choi, S., Lee, E. J., Shin, J. O., Park, E. Y., Bok, J., and Park, J. H. (2017) Profiling of miRNAs and target genes related to cystogenesis in ADPKD mouse models. *Sci Rep* **7**, 14151
15. Muto, Y., Dixon, E. E., Yoshimura, Y., Wu, H., Omachi, K., Ledru, N., Wilson, P. C., King, A. J., Eric Olson, N., Gunawan, M. G., Kuo, J. J., Cox, J. H., Miner, J. H., Seliger, S. L., Woodward, O. M., Welling, P. A., Watnick, T. J., and Humphreys, B. D. (2022) Defining cellular complexity in human autosomal dominant polycystic kidney disease by multimodal single cell analysis. *Nature Communications* **13**
16. Ransick, A., Lindström, N. O., Liu, J., Zhu, Q., Guo, J.-J., Alvarado, G. F., Kim, A. D., Black, H. G., Kim, J., and McMahon, A. P. (2019) Single-Cell Profiling Reveals Sex, Lineage, and Regional Diversity in the Mouse Kidney. *Developmental Cell* **51**, 399-413.e397
17. Chen, L., Clark, J. Z., Nelson, J. W., Kaissling, B., Ellison, D. H., and Knepper, M. A. (2019) Renal-Tubule Epithelial Cell Nomenclature for Single-Cell RNA-Sequencing Studies. *J Am Soc Nephrol* **30**, 1358-1364
18. Harris, P. C., and Torres, V. E. (2009) Polycystic kidney disease. *Annu Rev Med* **60**, 321-337
19. Devuyst, O., Burrow, C. R., Smith, B. L., Agre, P., Knepper, M. A., and Wilson, P. D. (1996) Expression of aquaporins-1 and -2 during nephrogenesis and in autosomal dominant polycystic kidney disease. *Am J Physiol* **271**, F169-183
20. Smith, A. O., Jonassen, J. A., Preval, K. M., Davis, R. J., and Pazour, G. J. (2021) c-Jun N-terminal kinase (JNK) signaling contributes to cystic burden in polycystic kidney disease. *PLoS Genet* **17**, e1009711
21. Ruiter, F. A. A., Morgan, F. L. C., Roumans, N., Schumacher, A., Slaats, G. G., Moroni, L., LaPointe, V. L. S., and Baker, M. B. (2022) Soft, Dynamic Hydrogel Confinement Improves Kidney Organoid Lumen Morphology and Reduces Epithelial-Mesenchymal Transition in Culture. *Adv Sci (Weinh)* **9**, e2200543
22. Kunnen, S. J., Malas, T. B., Formica, C., Leonhard, W. N., t Hoen, P. A. C., and Peters, D. J. M. (2018) Comparative transcriptomics of shear stress treated Pkd1(-/-) cells and pre-cystic kidneys reveals pathways involved in early polycystic kidney disease. *Biomed Pharmacother* **108**, 1123-1134
23. Zhang, C., Balbo, B., Ma, M., Zhao, J., Tian, X., Kluger, Y., and Somlo, S. (2021) Cyclin-Dependent Kinase 1 Activity Is a Driver of Cyst Growth in Polycystic Kidney Disease. *J Am Soc Nephrol* **32**, 41-51
24. Lipinski, M., Parks, D. R., Rouse, R. V., and Herzenberg, L. A. (1981) Human trophoblast cell-surface antigens defined by monoclonal antibodies. *Proc Natl Acad Sci U S A* **78**, 5147-5150
25. Shvartsur, A., and Bonavida, B. (2015) Trop2 and its overexpression in cancers: regulation and clinical/therapeutic implications. *Genes Cancer* **6**, 84-105

26. Trerotola, M., Cantanelli, P., Guerra, E., Tripaldi, R., Aloisi, A. L., Bonasera, V., Lattanzio, R., de Lange, R., Weidle, U. H., Piantelli, M., and Alberti, S. (2013) Upregulation of Trop-2 quantitatively stimulates human cancer growth. *Oncogene* **32**, 222-233
27. Qiu, S., Zhang, J., Wang, Z., Lan, H., Hou, J., Zhang, N., Wang, X., and Lu, H. (2023) Targeting Trop-2 in cancer: Recent research progress and clinical application. *Biochim Biophys Acta Rev Cancer* **1878**, 188902
28. Wang, J., Zhang, K., Grabowska, D., Li, A., Dong, Y., Day, R., Humphrey, P., Lewis, J., Kladney, R. D., Arbeit, J. M., Weber, J. D., Chung, C. H., and Michel, L. S. (2011) Loss of Trop2 promotes carcinogenesis and features of epithelial to mesenchymal transition in squamous cell carcinoma. *Mol Cancer Res* **9**, 1686-1695
29. Kaza, H., Barik, M. R., Reddy, M. M., Mittal, R., and Das, S. (2017) Gelatinous drop-like corneal dystrophy: a review. *Br J Ophthalmol* **101**, 10-15
30. Nakatsukasa, M., Kawasaki, S., Yamasaki, K., Fukuoka, H., Matsuda, A., Tsujikawa, M., Tanioka, H., Nagata-Takaoka, M., Hamuro, J., and Kinoshita, S. (2010) Tumor-associated calcium signal transducer 2 is required for the proper subcellular localization of claudin 1 and 7: implications in the pathogenesis of gelatinous drop-like corneal dystrophy. *Am J Pathol* **177**, 1344-1355
31. Ripani, E., Sacchetti, A., Corda, D., and Alberti, S. (1998) Human Trop-2 is a tumor-associated calcium signal transducer. *Int J Cancer* **76**, 671-676
32. Guerra, E., Trerotola, M., Tripaldi, R., Aloisi, A. L., Simeone, P., Sacchetti, A., Relli, V., D'Amore, A., La Sorda, R., Lattanzio, R., Piantelli, M., and Alberti, S. (2016) Trop-2 Induces Tumor Growth Through AKT and Determines Sensitivity to AKT Inhibitors. *Clin Cancer Res* **22**, 4197-4205
33. Lenart, S., Lenart, P., Smarda, J., Remsik, J., Soucek, K., and Benes, P. (2020) Trop2: Jack of All Trades, Master of None. *Cancers (Basel)* **12**
34. Zhao, W., Jia, L., Kuai, X., Tang, Q., Huang, X., Yang, T., Qiu, Z., Zhu, J., Huang, J., Huang, W., and Feng, Z. (2019) The role and molecular mechanism of Trop2 induced epithelial-mesenchymal transition through mediated beta-catenin in gastric cancer. *Cancer Med* **8**, 1135-1147
35. Saadi-Kheddouci, S., Berrebi, D., Romagnolo, B., Cluzeaud, F., Peuchmaur, M., Kahn, A., Vandewalle, A., and Perret, C. (2001) Early development of polycystic kidney disease in transgenic mice expressing an activated mutant of the beta-catenin gene. *Oncogene* **20**, 5972-5981
36. Hayashi, S., and McMahon, A. P. (2002) Efficient recombination in diverse tissues by a tamoxifen-inducible form of Cre: a tool for temporally regulated gene activation/inactivation in the mouse. *Dev Biol* **244**, 305-318
37. Badea, T. C., Wang, Y., and Nathans, J. (2003) A noninvasive genetic/pharmacologic strategy for visualizing cell morphology and clonal relationships in the mouse. *J Neurosci* **23**, 2314-2322
38. Sadate-Ngatchou, P. I., Payne, C. J., Dearth, A. T., and Braun, R. E. (2008) Cre recombinase activity specific to postnatal, premeiotic male germ cells in transgenic mice. *Genesis* **46**, 738-742

39. Jonassen, J. A., San Agustin, J., Follit, J. A., and Pazour, G. J. (2008) Deletion of IFT20 in the mouse kidney causes misorientation of the mitotic spindle and cystic kidney disease. *J Cell Biol* **183**, 377-384
40. Yukselen, O., Turkyilmaz, O., Ozturk, A. R., Garber, M., and Kucukural, A. (2020) DolphinNext: a distributed data processing platform for high throughput genomics. *BMC Genomics* **21**, 310
41. Bray, N. L., Pimentel, H., Melsted, P., and Pachter, L. (2016) Near-optimal probabilistic RNA-seq quantification. *Nat Biotechnol* **34**, 525-527
42. Love, M. I., Huber, W., and Anders, S. (2014) Moderated estimation of fold change and dispersion for RNA-seq data with DESeq2. *Genome Biol* **15**, 550
43. Chen, Y., Chen, Y., Shi, C., Huang, Z., Zhang, Y., Li, S., Li, Y., Ye, J., Yu, C., Li, Z., Zhang, X., Wang, J., Yang, H., Fang, L., and Chen, Q. (2018) SOAPnuke: a MapReduce acceleration-supported software for integrated quality control and preprocessing of high-throughput sequencing data. *Gigascience* **7**, 1-6
44. Muller, S., Rycak, L., Winter, P., Kahl, G., Koch, I., and Rotter, B. (2013) omiRas: a Web server for differential expression analysis of miRNAs derived from small RNA-Seq data. *Bioinformatics* **29**, 2651-2652
45. Langmead, B., Trapnell, C., Pop, M., and Salzberg, S. L. (2009) Ultrafast and memory-efficient alignment of short DNA sequences to the human genome. *Genome Biol* **10**, R25
46. Friedlander, M. R., Mackowiak, S. D., Li, N., Chen, W., and Rajewsky, N. (2012) miRDeep2 accurately identifies known and hundreds of novel microRNA genes in seven animal clades. *Nucleic Acids Res* **40**, 37-52
47. Anders, S., and Huber, W. (2010) Differential expression analysis for sequence count data. *Genome Biol* **11**, R106
48. Stuart, T., Butler, A., Hoffman, P., Hafemeister, C., Papalexi, E., Mauck, W. M., 3rd, Hao, Y., Stoeckius, M., Smibert, P., and Satija, R. (2019) Comprehensive Integration of Single-Cell Data. *Cell* **177**, 1888-1902 e1821
49. Edgar, R., Domrachev, M., and Lash, A. E. (2002) Gene Expression Omnibus: NCBI gene expression and hybridization array data repository. *Nucleic Acids Res* **30**, 207-210

Acknowledgements

We thank Dr. Owen M. Woodward from the Polycystic Kidney Disease Research Resource Consortium at the University of Maryland for sections of human kidney.

Funding

Work was supported by DK103632 and GM060992 to GJP. The content is solely the responsibility of the authors and does not necessarily represent the official views of the National Institutes of Health.

Ethics Statement

Mouse studies were approved by the Institutional Animal Care and Use Committee of the University of Massachusetts Chan Medical School.

Human kidney tissue samples from nephrectomized kidneys were received from the Maryland PKD Research and Translational Core Center (part of the NIDDK U54 PKD-RRC). Human sample use was reviewed by the University of Maryland School of Medicine Institutional Review Board (IRB) and determined not to be human research, requiring no further IRB review. Thus, the Ethics Committee/IRB of the University School of Medicine waived ethical approval of this work.

Author contributions

Abigail O. Smith: Conceptualization, Investigation, Data Curation, Formal analysis, Writing - Original Draft, Writing - Review & Editing

William Tyler Frantz: Conceptualization, Investigation, Data Curation, Formal analysis, Writing - Original Draft, Writing - Review & Editing

Kenley M. Preval: Conceptualization, Investigation, Formal analysis, Writing - Original Draft, Writing - Review & Editing

Yvonne J.K. Edwards: Conceptualization, Investigation, Data Curation, Formal analysis, Writing - Review & Editing

Craig J. Ceol: Writing - Review & Editing, Funding acquisition

Julie A. Jonassen: Conceptualization, Investigation, Formal analysis, Writing - Original Draft, Writing - Review & Editing, Funding acquisition

Gregory J. Pazour: Conceptualization, Investigation, Formal analysis, Writing - Original Draft, Writing - Review & Editing, Funding acquisition

Conflict of interest

The authors declare that they have no conflicts of interest with the contents of this article.

Data and materials availability

The data discussed in this publication have been deposited in NCBI's Gene Expression Omnibus (49) and are accessible through GEO Series accession numbers:

GSE222610 (https://www.ncbi.nlm.nih.gov/geo/query/acc.cgi?acc=GSE222610)

GSE220322 (https://www.ncbi.nlm.nih.gov/geo/query/acc.cgi?acc=GSE220322).

Reviewer token for miRNA (GSE222610) is idubgqkedfexraz and for mRNA (GSE220322) is ifoniomibbshbkb.